

# SARS-CoV-19-associated Rhino-orbital and cerebral mucormycosis: clinical and radiological presentations

Ashima Mittal <sup>1</sup>, Nitika Mahajan <sup>2</sup>, Devinder Pal Singh Dhanota <sup>1</sup>, Birinder S. Paul <sup>2</sup>, Srishti Ahluwalia <sup>3</sup>, Saumya Ahluwalia <sup>3</sup>, Arnav Galhotra <sup>3</sup>, Veenu Gupta <sup>4</sup>, Sanjeev Puri <sup>5</sup>, Rohit Verma <sup>5</sup>, Manish Munjal <sup>5</sup>, Sahil Goel <sup>6</sup>, Sumeet Chopra <sup>6</sup>, Rajesh Mahajan <sup>7</sup>, Archana Ahluwalia <sup>1</sup>, Kavita Sagar <sup>1</sup> and Gagandeep Singh <sup>1,2,8,\*</sup>

<sup>1</sup>Department of Radiodiagnosis and Imaging, Dayanand Medical College and Hospital, Ludhiana, Punjab, 141001, India

<sup>2</sup>Department of Neurology, Dayanand Medical College and Hospital, Ludhiana, Punjab, 141001, India

<sup>3</sup>MBBS Students, Dayanand Medical College and Hospital, Ludhiana, Punjab, 141001, India

<sup>4</sup>Department of Microbiology, Dayanand Medical College and Hospital Ludhiana, Punjab, 141001, India

<sup>5</sup>Department of Otorhinolaryngology, Dayanand Medical College and Hospital Ludhiana, Punjab, 141001, India

<sup>6</sup>Department of Ophthalmology, Dayanand Medical College and Hospital Ludhiana, Punjab, 141001, India

<sup>7</sup>Department of Internal Medicine, Dayanand Medical College and Hospital Ludhiana, Punjab, 141001, India

<sup>8</sup>University College London Hospitals Biomedical Research Centre, National Institute for Health Research, Queen Square Institute of Neurology, London, UK

\*To whom correspondence should be addressed. Dr. Gagandeep Singh, MD, Department of Neurology, Dayanand Medical College and Hospital, Ludhiana, Punjab 141001, India. Tel: 9815500720; E-mail: [g.singh@ucl.ac.uk](mailto:g.singh@ucl.ac.uk)

## Abstract

We describe presenting clinical and imaging manifestations of severe acute respiratory syndrome coronavirus-2 (SARS-CoV-2)-associated Rhino-oculo-cerebral mucormycosis (ROCM) in a hospital setting during the second wave of SARS-CoV-2 pandemic in India. Data on the presenting manifestations were collected from 1 March to 31 May 2021. Associations between clinical and imaging findings were explored, specifically: (1) the presence or absence of orbital pain and infiltration of a superior orbital fissure on imaging; (2) the presence of unilateral facial nerve palsy and pterygopalatine fossa infiltration and geniculate ganglion signal on contrast magnetic resonance imaging, and (3) vision loss and optic nerve findings on imaging. Orbital pain was reported by 6/36 subjects. A fixed, frozen eye with proptosis and congestion was documented in 26 (72%), complete vision loss in 23 (64%), and a unilateral lower motor neuron facial nerve palsy in 18 (50%). No association was found between the presence of orbital pain and superior orbital fissure infiltration on imaging. The ipsilateral geniculate ganglion was found to enhance more profoundly in 7/11 subjects with facial palsy and available magnetic resonance (MR) imaging, and the ipsilateral pterygopalatine fossa was found infiltrated in 14. Among 23 subjects with complete loss of vision, 9 (39%) demonstrated long-segment bright signal in the posterior optic nerve on diffusion MR images. We conclude that orbital pain might be absent in SARS-CoV-2-associated ROCM. Facial nerve palsy is more common than previously appreciated and ischemic lesions of the posterior portion of the optic nerve underlie complete vision loss.

## Lay summary

Unique clinical and radiological manifestations identified in the outbreak of Rhino-oculo-cerebral mucormycosis (ROCM) during the second epidemic wave of coronavirus disease 2019 (COVID-19) infection included the common occurrence of facial paralysis, frequent absence of ocular pain, and long segments of optic nerve damage.

**Keywords:** fungal infection, sinusitis, cerebral infarcts, cavernous sinuses, superior orbital fissure

## Introduction

Rhino-oculo-cerebral mucormycosis (ROCM), an uncommon disorder, denotes fungal infection of the nasal and paranasal cavities, eyes, and brain with spores of *Mucor*, *Rhizopus*, *Cunninghamella*, *Lichthemia*, and *Apophysomyces*.<sup>1</sup> Once the spores lodge in the nasal mucosa leading to necrosis, local symptoms occur in the form of nasal stuffiness and sometimes, a bloody discharge. The fungus is highly angio-invasive and it spreads from the nose to the paranasal sinuses, orbits, cavernous sinuses, meninges, and brain. The skin overlying the paranasal sinuses and soft tissues in the infratemporal fossae are often affected. The most common risk factor for ROCM is diabetes mellitus, when uncontrolled including diabetic

ketoacidosis. Other risk factors include hematological malignancies, bone marrow or solid organ transplant recipients, iron overload states, and immunosuppression from corticosteroid use.<sup>2</sup>

Globally, ROCM is rare, as a laboratory-based population survey in 1992–1993 from California estimated a prevalence of 2/1 000 000.<sup>3</sup> The global incidence has likely increased recently because of an increasing use of corticosteroids and the occurrence of neutropenia, for instance in acute myeloid leukemia. The estimated burden in India is about 70 times the global prevalence.<sup>4</sup> Most infections are sporadic, but outbreaks occasionally occur, mostly during natural disasters. A large, nationwide outbreak occurred in India during the second epidemic wave of SARS-CoV-2 infection.<sup>5</sup> As the

SARS-CoV-2 infections peaked during the first week of May 2021, large numbers of ROCM cases were reported from across the country. The Government of India responded by declaring mucormycosis as a notifiable disease but was confronted by a cataclysmic shortage of amphotericin B, the core ingredient in the therapeutic armamentarium against ROCM. By June 16, there were 27 000 cases of ROCM.<sup>6</sup> The challenge was to develop and implement diagnostic protocols in the presence of the ongoing SARS-CoV-2 pandemic and the non-availability of amphotericin B. Besides India, SARS-CoV-2 associated ROCM was reported, albeit anecdotally, from several countries, including the United States, Brazil, Iran, and Egypt.<sup>7-9</sup> Here, we report our experience in terms of some novel and unusual clinical and radiological presenting manifestations of COVID-19-associated ROCM in a cohort of patients from a single center. The outcome and experience with the treatment are being analyzed separately as part of a multicenter collaborative undertaking across India. Specifically, we sought to determine an association between certain clinical findings and radiological markers, i.e., (1) the presence or not of orbital pain and infiltration of superior orbital fissure; (2) identification of a unilateral facial palsy and infiltration of ipsilateral pterygopalatine fossa and an abnormal ipsilateral geniculate ganglion signal; and (3) vision loss and findings on imaging of optic nerves.

## Methods

We prospectively collected data on the presenting clinical and imaging manifestations of people admitted with a presumed diagnosis of ROCM to Dayanand Medical College and Hospital, Ludhiana over a period of 3 months (1 March–31 May 2021) during the second wave of the SARS-CoV-2 pandemic in India. The study was approved by the Institutional Ethics Committee. All subjects gave informed consent for participation.

**Clinical assessments:** Detailed general, physical, systemic, neurological, ophthalmologic, and otolaryngologic examinations were performed by the concerned specialists after admission. The otolaryngology team performed a local examination with a nasal endoscope (Karl Storz endoscope; 4 mm, 8 cm size, Tuttlingen, Germany) for the presence of nasal or palatal crusts, ulcers, and hypertrophied turbinates. Nasal scrapings from suspicious sites and any discharge when issuing was collected and examined for fungal hyphae using potassium hydroxide (KOH) preparation and calcofluor white stain. Routine laboratory investigations included complete blood counts, renal and liver biochemical analyses, blood sugars and glycosylated hemoglobin levels, and chest roentgenograms and electrocardiograms. Material from throat or nasal swabs were examined for SARS-CoV-2 by reverse transcriptase polymerase chain reaction (RT-PCR) (TRUPCR SARS-CoV-2 RT q PCR KIT; V-3.2, 3B Blackbio Biotech India Ltd., Bhopal, India) method. Anti-SARS-CoV-2 antibodies were also (immuno-) assayed in Beckman coulter machines (Access SARS-CoV-2 IgG, Washington DC, USA). Subjects who were SARS-CoV-2 RT-PCR-positive underwent computed tomography (CT) of the paranasal sinuses, orbits, and brain and were managed in a SARS-CoV-2 isolation ward. Elsewise, they underwent MR imaging of brain, orbit, and paranasal sinuses and were managed in a purpose-made multidisciplinary mucor ward.

**Clinical variables:** Findings recorded on physical examination included unilateral or bilateral facial swelling, and unilateral or bilateral ocular congestion, conjunctival edema, proptosis, and peri-orbital swelling. Proptosis was confirmed by the worm's eye view approach and although, it was not measured, an attempt was made to determine its direction as well as vertical displacement of the globe. It was regarded as axial when the axis of the eye was maintained whilst looking ahead. When displaced horizontally or vertically, the direction of its displacement was noted. Ophthalmoplegia or paresis was classified as fixed and complete, in which case the eye was immovable and the pupil, non-reactive and partial when some movement of the eye was observed. Bedside ophthalmoscopy (Heine Omega 500 Indirect Ophthalmoscope, Gilching, Germany) was performed by ophthalmologists unless precluded by corneal edema or concerns of COVID-19 infectivity. Paranasal sinus assessment included examination using a fiberoptic nasal endoscope (Karl Storz endoscope; 4 mm, 8 cm size, Germany). During this exam, crusts and secretions were taken for direct microscopic examination using wet KOH mount and/or calcofluor staining in which tissue was dissolved in a tube of 10/20% KOH without centrifugation or grinding the sample.<sup>10</sup>

**Imaging protocols:** Computed tomography (CT) was performed on a Siemens scanner (Somatom Definition, AS 128 slice Siemens Medical System, Erlangen, Germany; 120 kVP and 150–220 mA tube current). The paranasal sinus protocol included imaging of paranasal sinuses with orbits, repeated after administration of intravenous contrast (low osmolar, non-ionic, 300 mg/ml iodine content; dose 1 ml/kg) pushed by a pressure injector. Images were acquired at 0.625 mm slice thickness and reconstructed to obtain 1 mm thick slices in axial, sagittal, and coronal planes. MR images were acquired on a Siemens (Magnetom Skyra; Erlangen, Germany) 3 Tesla scanner with a 20-channel head coil. The brain, orbit, and paranasal sinuses were imaged, including axial and coronal T1 weighted (TR/TE: 780/17 ms; slice thickness 3 mm; number of slices, 25; field of view [FOV], 180 mm; matrix, 320; number of excitations i.e., NEX 2), axial, sagittal, coronal, T2-weighted images with and without fat saturation (TR/TE 6120/90 ms; slice thickness, 3 mm; number of slices, 25; FOV, 180 mm; matrix, 320; NEX 2), Dixon axial T2 fat saturation sequences (TR/TE 1180/72 ms; slice thickness, 3 mm; number of slices, 25; FOV, 180 mm; matrix, 320; NEX 2), diffusion-weighted imaging (DWI), susceptibility weighted imaging (SWI), fat-suppressed post-contrast T1 weighted images (TR/TE 780/17 ms; slice thickness, 3 mm; number of slices, 25; FOV, 180; matrix, 320; NEX 2) and T1 SPACE post-contrast (TR/TE 700/11 ms; slice thickness, 1 mm; number of slices, 192/slab; FOV, 220 mm; matrix, 256; NEX 2) sequences.

**Image interpretation and imaging variables:** A stepwise approach was followed in the interpretation of contrast-enhanced CT and/or MR images of the nasal cavity, paranasal sinuses, orbits, and intracranial structures. First, mucosal and turbinate hypertrophy in the nasal cavity and partial or complete opacification of the paranasal sinuses were noted on CT and/or MR images. Mucosal hypertrophy and hyperdense contents within nasal cavity and paranasal sinuses on CT denoted fungal sinusitis. Contrast enhancement of the mucosa was classified as none, mild, or heterogeneous.<sup>11</sup> On magnetic resonance T2 weighted (MR T2) images, sino-nasal mucosal hypertrophy was likewise characterized and could be hyperintense or heterogeneous, i.e., mixed

with hypo- and hyper-intensities within. Diffusion restriction within the hypertrophied mucosa implied necrosis. Post-contrast MR images were examined for rim-like enhancement with a central non-enhancing core or heterogenous enhancement within the thickened mucosa. Hypertrophied sino-nasal mucosa, appearing heterogenous on T2 images, with diffusion restriction on diffusion weighted imaging/apparent diffusion coefficient (DWI/ADC) and rim enhancement with a central non-enhancing core denoted either necrotic or infarcted material. Increased density of fat on CT or increased intensity of fat on MR fat-saturated sequences in the involved regions denoted fat stranding.

Features indicative of orbital cellulitis included soft tissue infiltration/stranding in the intraconal and extraconal fat, bulky extraocular muscles, and a thrombosed or engorged superior ophthalmic vein (characterized by the loss of flow void on fat-saturated T2 images), with exophthalmos and pre-septal edema. Two varieties of abnormalities of the optic nerve were identified on MR images. A thickened appearance, hyperintense on T2 images, with diffusion restriction on DWI/ADC, and absence of enhancement within the nerve on post-contrast images indicated ischemic optic neuropathy. The length of the infarcted segment on axial images was noted. Enhancement of the optic nerve sheath on axial and coronal post-contrast images suggested optic perineuritis.<sup>12</sup>

The superior orbital fissure (SOF) and orbital apex were examined for soft tissue infiltration and fat stranding on axial and coronal T2 fat-saturated and post-contrast MR images. In addition, the SOF was partitioned into superolateral and the intra-annular middle parts and the presence of infiltrates and necrosis in the two parts was assessed. The extra-annular superolateral part is separated from the orbital apex by the optic strut posteriorly and tendinous annulus of Zinn, which is the origin of most extra-ocular muscles. It transmits the lacrimal, trochlear, and frontal nerves in addition to the superior ophthalmic vein. The intra-annular middle part encompasses the optic nerve, the superior and inferior divisions of the third nerve, and the nasociliary nerves. The superior ophthalmic vein was utilized as a landmark to partition the SOF. The orbital fat surrounding this vein represented the superolateral segment, while the orbital fat inferolateral to the optic nerve represented the middle intra-annular segment of the SOF on axial and coronal fat-saturated and post-contrast images. Orbital compartment syndrome was diagnosed in the presence of severe proptosis, tenting of the posterior globe, and stretching of the optic nerve either on CT or MR images.

The following features were consistent with a radiological label of cerebritis: ill-defined hypodense areas on CT; hyperintense areas on T2 weighted/fluid attenuated inversion recovery magnetic resonance (T2/FLAIR MR) images; diffusion restriction on DW/ADC images; foci of blooming (suggesting hemorrhage) on susceptibility weighted imaging (SWI) images; non- or minimally-enhancing lesions not conforming to cerebral vascular territories but adjacent to the involved sinuses. Lesions with similar characteristics but following the distribution of a vascular territory and located distant from a diseased sinus(es) were labeled as infarcts. Lesion(s) with a hyperintense core and hypointense rim on T2/FLAIR, and with peripheral diffusion restriction, blooming, and enhancement were regarded as fungal abscess(es). Focal or diffuse dural thickening and enhancement on MR images were considered indicative of pachymeningitis. Bulky cavernous sinus(es) with convex lateral margins and non-enhancing filling defects or soft tissue infiltration represented cavernous sinus thrombosis.

Additional features that indicated intracranial involvement included thrombosis of the cavernous segment of the internal carotid artery, characterized by a lack of enhancement and flow void, soft tissue extension to Meckel's cave, and the presence of epidural collections. In patients with or without facial palsy, the course of the seventh cranial nerve and its enhancing segments were noted on both sides on T1 sampling perfection with application optimised contrasts using different flip angle evolution (T1 SPACE) post-contrast sequences.<sup>13</sup> Asymmetry in the dimensions and intensity of enhancement of the geniculate ganglion were noted. Symmetrical enhancement of the geniculate ganglia on both sides was considered normal.

The pterygopalatine fossa was evaluated for soft tissue infiltration or fat stranding visible as heterogenous hyperintensities on T2 fat-saturated MR sequences. Besides, the masticator space, peri-antral (retro-antral and premaxillary), pre-zygomatic and buccal spaces were assessed for soft tissue extension and/or fat stranding and increased muscle bulk with the altered signal. Lastly, the presence of bone involvement was signaled by rarefaction, erosions, lytic destruction, and sclerosis on CT. Skull base osteomyelitis was distinguished by loss of normal T1 hyperintense signal with hyperintensity on T2 fat-saturated images of the bones forming the skull base.

*Clinical-imaging associations:* An association between complaints of orbital pain and the presence of infiltrates in the superolateral segment of the SOF outside of the annulus of Zinn versus the intra-annular, middle segment<sup>14</sup> using the superior ophthalmic vein as a landmark was studied. It was postulated that orbital pain would occur with involvement of the frontal nerve and its absence thereof would indicate sparing of the superolateral segment of the superior orbital fissure. Next, the occurrence and laterality of seventh cranial nerve palsy were compared with the dimensions and intensity of enhancement of the ipsilateral *vs.* contralateral geniculate ganglion, the presence of infiltrates and necrosis in the ipsilateral pterygopalatine fossa, and lytic bony destruction in the region of the facial canal. Lastly, the relationship of loss and scale (complete *vs.* partial) thereof vision with the presence of abnormal signals in diffusion-weighted images of the optic nerve was assessed.

## Results

The second peak of the SARS-CoV-2 epidemic in India occurred in early May 2021. Just about the same time, a substantial number of ROCM infections were reported across the country. By 17 June 2021, 27 000 cases were notified to the Government of India.<sup>6</sup> We report 36 cases (20 females [55%]; mean age: 58 years; range: 31–85 years) with evidence of ROCM on CT and/or MR imaging performed on admission to hospital with or without histopathological confirmation between 1 March 2021 and 31 May 2021. Prior diabetes mellitus was noted in 32 (89%), hypertension in 11 (31%), and cardiac disorders in 3 (8%) subjects. A total of 17 (47%) subjects were SARS-CoV-2 RT-PCR-positive upon admission, while 8 (22%) had documented COVID-19 in the preceding 2 months. Another 11 (30%) demonstrated anti-SARS-CoV-2 antibodies; of these 5 had prior infectious episodes compatible with COVID-19 but tested negative on the SARS-CoV-2 RT-PCR. A total of 9 (25%) among them had received the first dose of the SARS-CoV-2 vaccine. The mean duration of symptoms prior to admission was 5 days (range: 1–22 days; median: 5 days; interquartile range: 3–7 days).

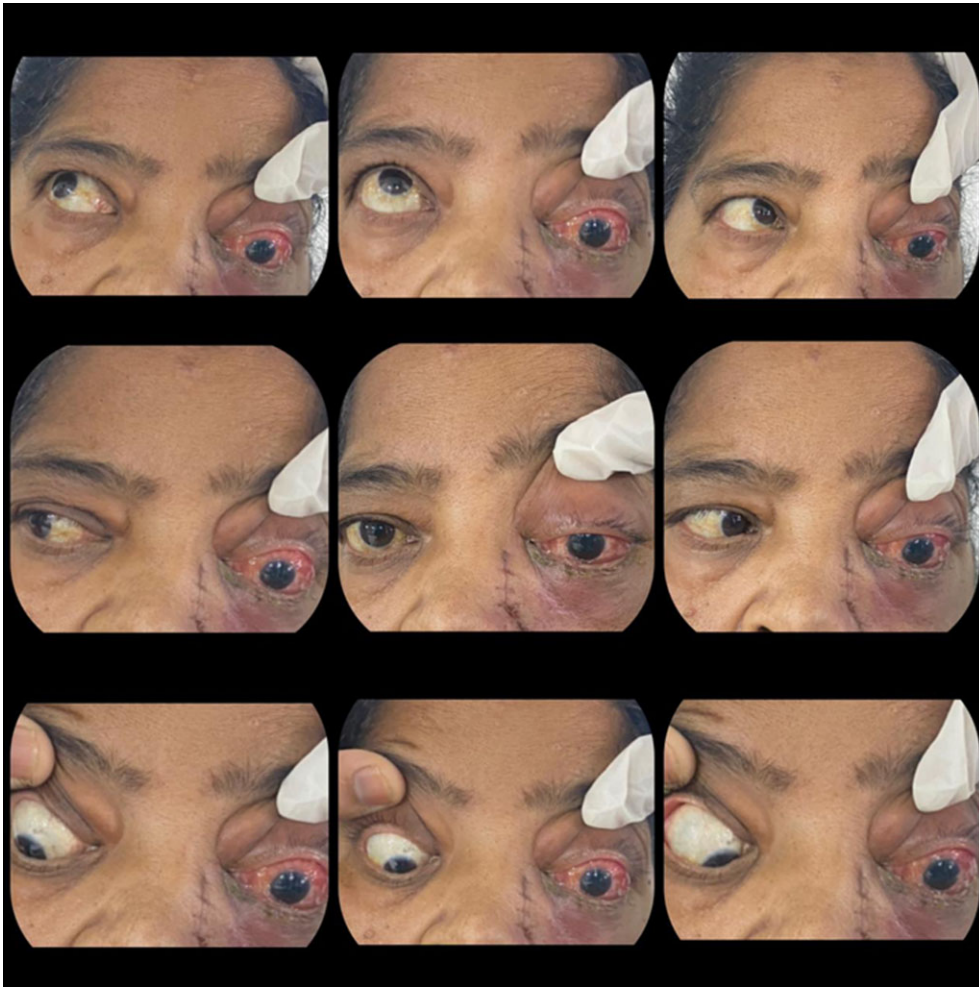


**Figure 1.** Eye movements in all eight cardinal directions depicting a fixed and immobile left eye in a subject with left orbital mucormycosis.

Of those with prior SARS-CoV-2 infection ( $n = 30$  with RT-PCR positivity in 25), 28 (78%) had used oral or intravenous corticosteroids and 18 (50%) had received oxygen support during active infection.

**Clinical findings:** Only six subjects complained of pain specifically over the orbital region; others complained of pain on presentation, located variously over the infra-orbital portion of the face on one or both sides ( $n = 8$ ) or headache ( $n = 4$ ). Orbital pain was conspicuous by its absence in 30 (83%) subjects. Unilateral complete ophthalmoplegia, i.e., a frozen eye with loss of pupillary light reflex, ptosis, proptosis, and conjunctival congestion was noted upon admission in 26 (72%) subjects (Fig. 1). Bilateral ophthalmoplegia (Fig. 2) and an isolated sixth cranial nerve palsy were encountered in 1 (3%) subject each. The proptosis was axially directed in 19, but was laterally-directed in 3 and the eye was vertically displaced in 4 subjects (Fig. 3a–d). Complete vision loss with absent light perception (bilateral in one and unilateral in the rest) was documented in 23 (64%), and partial unilateral vision loss in 4 (11%) subjects. Visual acuity was normal in the remainder. Central retinal artery occlusion was documented in 11 (48%) subjects with complete vision loss and in none of the 4 subjects with partial vision loss. No significant retinal changes were detected on indirect ophthalmoscopy in three subjects with complete vision loss. Severe corneal opacities or edema precluded assessment in two subjects. Ophthalmol-

oscopy could not be undertaken in the remainder including nine subjects with complete vision loss. Unilateral sensory loss in the distributions of the ophthalmic and maxillary divisions of the trigeminal nerve was documented in 11 (31%) subjects. The sensory loss was bilateral in one subject. An unambiguous unilateral lower motor neuron facial palsy was observed in 18 (50%) and bilateral in 1 subject (Fig. 4a–b). Facial edema precluded an assessment of facial paralysis in 5 (14%).

**Imaging findings:** MR imaging was performed in 20 (56%) patients with additional gadolinium-based contrast imaging in 16 (44%). CT was performed in 34 (94%) and with additional post-contrast exams in 11 (32%). Impaired renal function precluded contrast administration in the remainder.

Not one subject had disease confined to the nasal cavity alone on imaging. All demonstrated disease in the paranasal sinuses in addition to the nose. Further, the orbital extension was documented in 28 (78%) and intracranial extension in 16 (44%).

**Sino-nasal involvement:** The maxillary sinus was found involved in all cases (unilateral in 22; bilateral in 14) (Table 1). Other paranasal sinuses found involved were the anterior ethmoid/s in 35 (97%; unilateral in 15, bilateral in 20), posterior ethmoid/s in 32 (89%; unilateral in 16, bilateral in 16), sphenoid in 27 (75%; unilateral in 12, bilateral in 15) and frontal in 22 (61%; unilateral in 13, bilateral in 9) sinuses. A combination of maxillary, ethmoid, and sphenoid sinus



**Figure 2.** Bilateral complete ophthalmoplegia, in a subject with ROCM.

involvement was observed in 12 (33%). Pansinusitis was apparent in 6 (17%).

Hypertrophy of the nasal mucosa and turbinates was discernable in 29 (81%) cases. On CT, sino-nasal mucosal hypertrophy with hyperdense contents in the sinuses could be seen in 25 (74%) (Table 2). Mild enhancement of the nasal mucosa was observed in 6 (54%) and heterogenous enhancement in another 3 (27%) cases. The thickened mucosa was hypointense on T1-weighted images in all 20 cases, in whom MR was performed. On T2 images, however, a heterogenous pattern was identified in 19 (95%) and a pure hyperintense pattern in 1. Diffusion restriction within the hypertrophied mucosa was visualized in 16 (80%). A central non-enhancing core with rim enhancement was noted in 12 (75%) and heterogenous enhancement in 4 (25%) on post-contrast MR imaging. A combination of a heterogenous appearance on T2 images, diffusion restriction, and a central non-enhancing core with rim enhancement within the hypertrophied sino-nasal mucosa was noted in 15 (75%) (Fig. 5a–e, red arrows).

Bone changes on CT in the form of bone rarefaction, erosion, and permeating destruction were detected in 8 (22%) cases, of which, gross bony lysis or destruction was observed in only 2 and bony rarefaction in 6.

*Extension beyond paranasal sinuses:* Orbital involvement was present in the form of orbital cellulitis in 24 (67%)

(unilateral in 22 [61%] and bilateral in 2), optic peri-neuritis in 4 (20%), and posterior ischemic optic neuropathy (PION) in 14 (70%) (out of 20 patients who underwent MR imaging) (Table 3). The latter was characterized by T2 hyperintensity within the optic nerve in 12 (60%) cases, diffusion restriction in all 14 (70%), and absence of enhancement in 10 (50%) (Fig. 6a–f). Superior orbital fissure with orbital apex involvement was seen in 19/20 patients who underwent MRI. This was bilateral in one and unilateral in the remainder. Orbital compartment syndrome was diagnosed on the basis of characteristic imaging attributes in 2 (6%) (Fig. 5a).

Intracranial extension was demonstrated by findings of cerebritis in 4 (11%), infarcts in 6 (16.6%), an abscess in 1 (2.7%), cavernous sinus thrombosis in 7 (35%), internal carotid artery thrombosis in 1 (3%), extradural collections in 4 (11%) (Fig. 5a–d, white arrows), pachymeningitis in 5 (14%) (Fig. 5e–f, black arrows) and Meckel's cave infiltration in 4 (11%) (Fig. 5a–d, yellow arrows).

Soft tissue extension or fat stranding in pterygopalatine fossa was observed in 18/20 (90%) patients with MR imaging (Fig. 7a–d); of these, 14 (78%) had an ipsilateral facial palsy. Involvement of masticator space and peri-antral fat was observed in 20 (56%) cases. Skull base osteomyelitis was identified in 5 (14%) subjects.

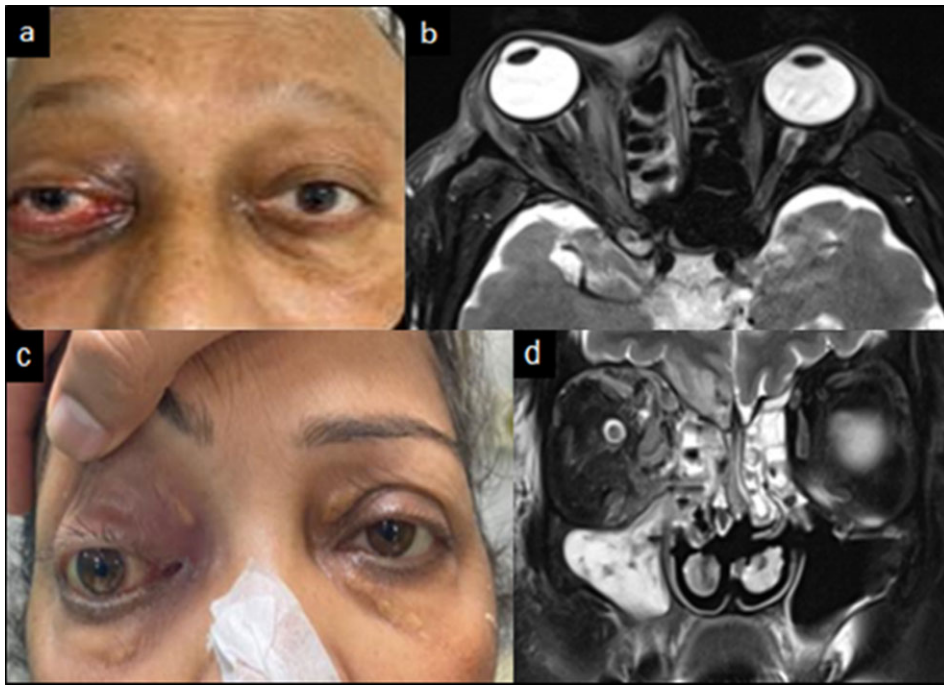


**Figure 3.** ROCM (a) Clinical photograph showing unilateral complete ophthalmoplegia with conjunctival congestion, and laterally directed proptosis in right eye. (b) Axial MRI T2 dixon fat sat image in patient (a) showing hyperintense mucosal hypertrophy in right ethmoid sinuses responsible for right lateral proptosis. (c) Clinical photograph post maxillectomy status, showing unilateral complete ophthalmoplegia and proptosis with downward displacement of the right eye. (d) Preoperative coronal MRI T2 fat sat image in patient (c) showing heterogeneously hyperintense mucosal hypertrophy in right maxillary and bilateral ethmoid sinuses, right intraorbital fat stranding with bulky extra-ocular muscles.

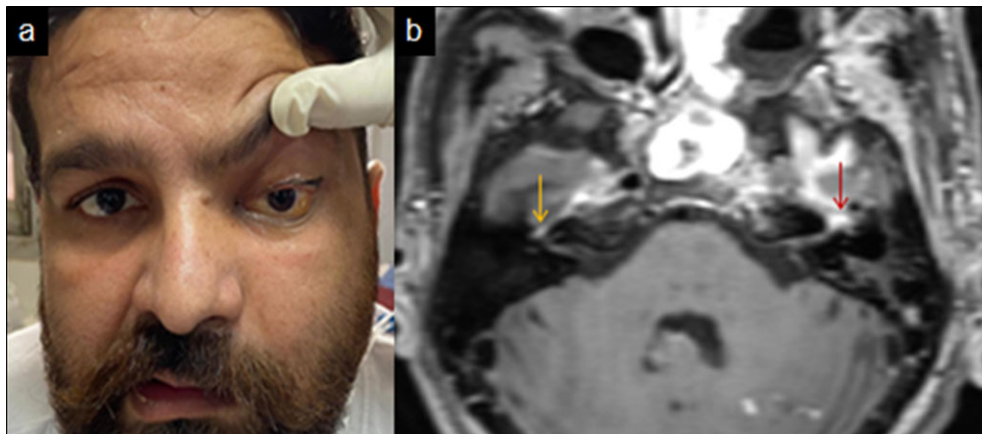


**Figure 4.** ROCM (a) Clinical photograph showing an obliterated nasolabial fold on the left side indicative of a lower motor neuron facial palsy on the left side (Note also an ophthalmoplegia and proptosis on the left side). (b) Axial post-contrast T1W fat-saturation MR image showing increase in size and intensity of enhancement of left geniculate ganglion (red arrow) relative to the right side (yellow arrow).

**Table 1.** Frequency of sinus involvement in mucormycosis.

Sinuses involved	Unilateral n (%)	Bilateral n (%)
Maxillary sinus	22 (61)	14(39)
Anterior Ethmoid sinus	15 (42)	20 (56)
Posterior Ethmoid sinus	16 (44)	16 (44)
Sphenoid sinus	12 (33)	15 (42)
Frontal sinus	13 (36)	9 (25)
Maxillary + Ethmoid sinuses	6 (17)	3 (8)
Maxillary + Ethmoid + Sphenoid sinuses	6 (17)	6 (17)

**Clinical and imaging correlation:** Of 6 patients, who complained of orbital pain, MR imaging was undertaken in 3; the superolateral segment of the SOF was infiltrated in all 3 with additional orbital apex disease in another 2 (Figs. 8 and 9). Of the 30 subjects who did not complain of orbital pain on presentation, 17 (57%) underwent MR imaging. Among them, the middle intraconal segment of the SOF and orbital apex were found infiltrated in 16 (94%) and the superolateral segment was infiltrated in 11 (65%). No association was found between the complaints of orbital pain and the identification of disease in the superolateral segment of the superior orbital fissure. Secondly, of the 19 subjects with lower motor neuron facial palsy, post-contrast MR images of the geniculate ganglia were available in 11. In seven, a distinct

**Table 2.** CT and MR features of sino-nasal mucosal thickening.

CT features	Number (%)	MR features	Number (%)
Mucosal thickening with hyperdense contents	25 (74)	T1W Signal Hypointense	20 (100)
Enhancement pattern of mucosa		T2W Signal	
None	2 (18)	Heterogenous	19 (95)
Mild	6 (54)	Hyperintense	1 (5)
Heterogenous	3 (27)	Diffusion restriction	16 (80)
		Enhancement pattern of mucosa	
		Central non enhancement with rim enhancement	12 (75)
		Heterogenous	4 (25)

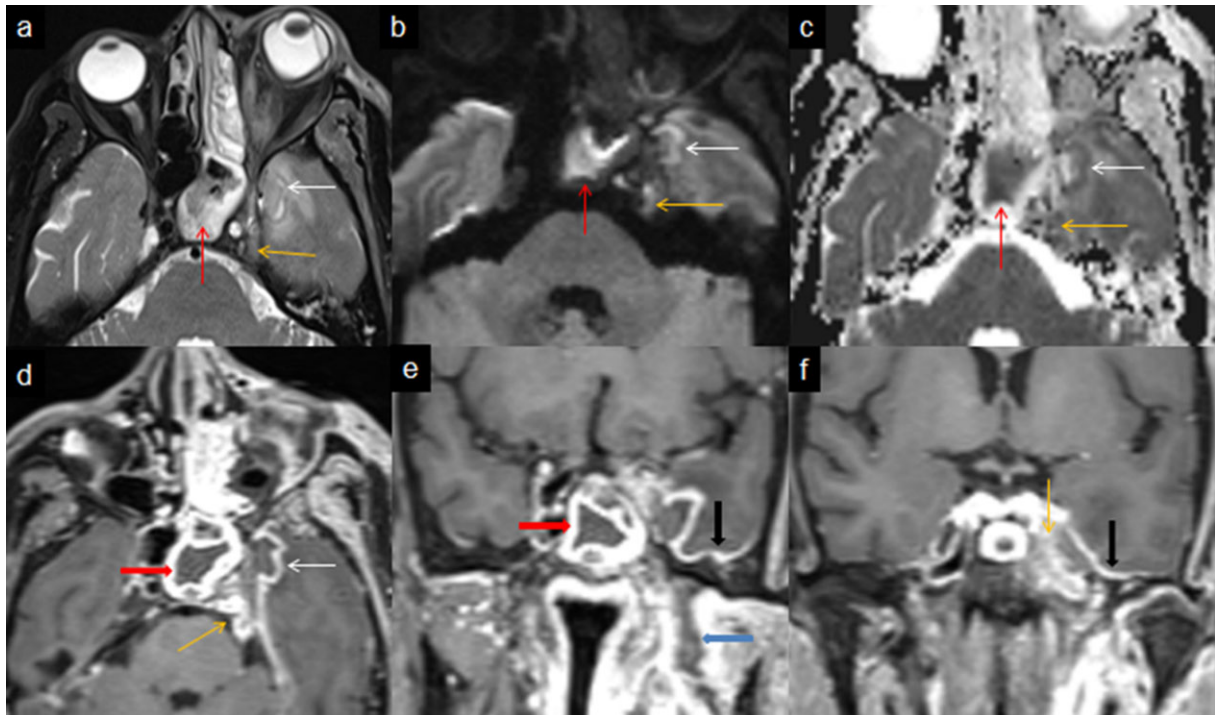


**Figure 5.** ROCM with left ophthalmoplegia showing constellation of imaging findings in a single case. (a) Red arrows showing heterogenous mucosal hypertrophy with hypointense contents in left sphenoid sinus on axial T2 fat saturated image, which show (b–c) diffusion restriction on DW/ADC, and (d–e) central non-enhancing mucosa with rim enhancement suggestive of necrosis on axial and coronal T1 post contrast images. Note also the ptosis in left eye with posterior tenting of eye globe s/o orbital compartment syndrome in (a). Yellow arrows show iso- to hypo-intense soft tissue in left Meckel’s cave (a), which shows diffusion restriction (b–c), and intense heterogenous enhancement of soft tissue in left Meckel’s cave with thickening and enhancement of cisternal part of left trigeminal nerve (d and f). White arrows show a small hyperintense extraaxial collection in left temporal region (a), which shows peripheral diffusion restriction (b–c), and peripheral enhancement (d). Black arrows show thick pachymeningeal enhancement along floor of middle cranial fossa on left side (e–f). Blue arrow in (e) shows non-enhancing soft tissue along the course of mandibular division of left trigeminal nerve suggestive of abscess formation.

asymmetry with greater size and intensity of enhancement of the geniculate ganglion on the side of the facial palsy was seen, including one subject with bilateral facial nerve palsies. In three of the subjects without evidence of facial palsy on initial clinical examination, post-contrast MR images showed faint but fairly symmetrical enhancement of both geniculate ganglia. Of note, 14 (78%) out of 18 subjects with unilateral pterygopalatine fossa involvement had a clinically detected ipsilateral lower motor neuron facial palsy. Lastly, of 23 patients with complete vision loss, 11 (48%) were diagnosed with central retinal artery occlusion on the basis of fundoscopic examinations. Diffusion restriction within long segments of the ipsilateral optic nerve but sparing the anterior-most

portion was observed in 9 cases (39%). MR exams could not be undertaken in the remaining two. Three patients with complete loss of vision had no evidence of central retinal artery occlusion on fundus exam; diffusion restriction was identified within the optic nerve in one. One patient with partial vision loss also demonstrated a constellation of imaging findings consistent with posterior ischemic optic neuropathy.

*Diagnostic confirmation and outcome:* A presumptive diagnosis was established through tissue biopsy in 16 (44%) patients, and KOH smear in 20 (55%). The KOH smear demonstrated hyaline aseptate fungal hyphae in 18, hyaline septate hyphae in 4, both aseptate and septate hyphae in 3, and no fungal elements in 3 subjects. Tissue biopsy revealed

**Table 3.** Frequency of involvement of sites beyond paranasal sinuses.

Sites of involvement beyond paranasal sinuses		Number (%)	
Orbit	Orbital cellulitis	24/36 (67)	
		Bilateral Unilateral	2/36 (6) 22/36 (61)
	Optic perineuritis	4/20 (20)	
		Posterior ischemic optic neuropathy	14/20 (70)
	Superior orbital fissure	T2 Hyperintensity	12/20 (60)
		Diffusion restriction	14/20 (70)
		No post contrast enhancement	10/20 (50)
	Orbital compartment syndrome	19/20 (95)	
		2/36 (6)	
	Intracranial	Cerebritis	4/36 (11)
Infarcts		6/36 (16.6)	
Abscesses		1/36 (2.7)	
Cavernous sinus thrombosis		7/20 (35)	
ICA Thrombosis		1/36 (3)	
Extra-axial collection/abscess		4/36 (11)	
Pachymeningitis		5/36 (14)	
Meckel cave		4/36 (11)	
7th nerve involvement		7/11 (64)	
		Bilateral Unilateral	1/11 (9) 6/11 (55)
Infratemporal fossa	Masticator space	20/36 (56)	
	Pterygopalatine fossa	18/20 (90)	
Osseous	Osseous	8/36 (22)	
	Skull base osteomyelitis	5/36 (14)	

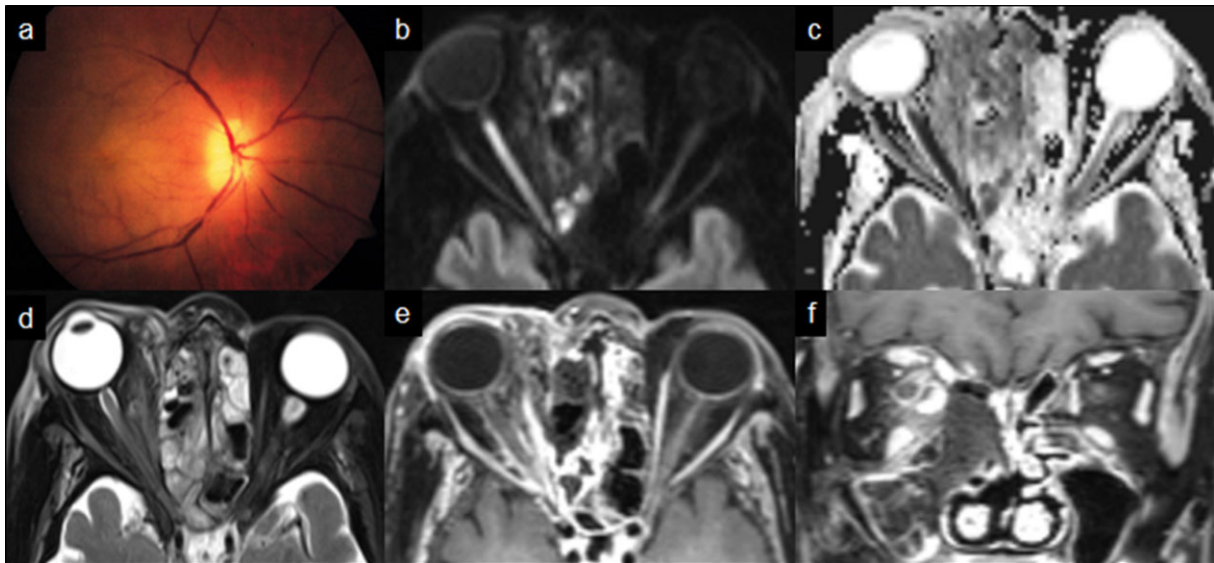


**Figure 6.** ROCM with complete vision loss in right eye (a) Fundus photograph demonstrating central retinal artery occlusion with cattle tracking of retinal arterioles and optic disc edema; (b) Axial diffusion weighted (DW) and (c) ADC MR images showing marked diffusion restriction in the intraorbital segment of right optic nerve (note also the diffusion restriction in the hypertrophied right ethmoid mucosa); (d) Axial T2 Dixon fat saturation MR image showing hyperintensity and thickening of the right optic nerve (note also the heterogeneous mucosal hypertrophy in both ethmoid sinuses and fat stranding in the right orbit); (e) Axial, and (f) Coronal T1 fat-saturation post-contrast MR images showing enhancement and thickening of the optic nerve sheath on right side suggestive of optic perineuritis. (Note the absence of enhancement within the optic nerve.) (Note also the non-enhancing mucosa in the right ethmoid and maxillary sinuses indicative of necrosis and the bulky extraocular muscles in the right orbit.)

zygomycosis in 13 subjects. A total of 10 (28%) subjects died in hospital, 5 (14%) were discharged against medical advice, and the remainder (58%) were discharged otherwise. Of the latter, 10 (39%) were not available for follow-up, 6 (23%) died, and 10 (39%) eventually improved.

## Discussion

ROCM is an uncommon disorder; hence, its clinical imaging findings have been mostly described in only isolated reports or small series of cases.<sup>11</sup> Besides, although a handful of large series of cases are available, these have reported only broad

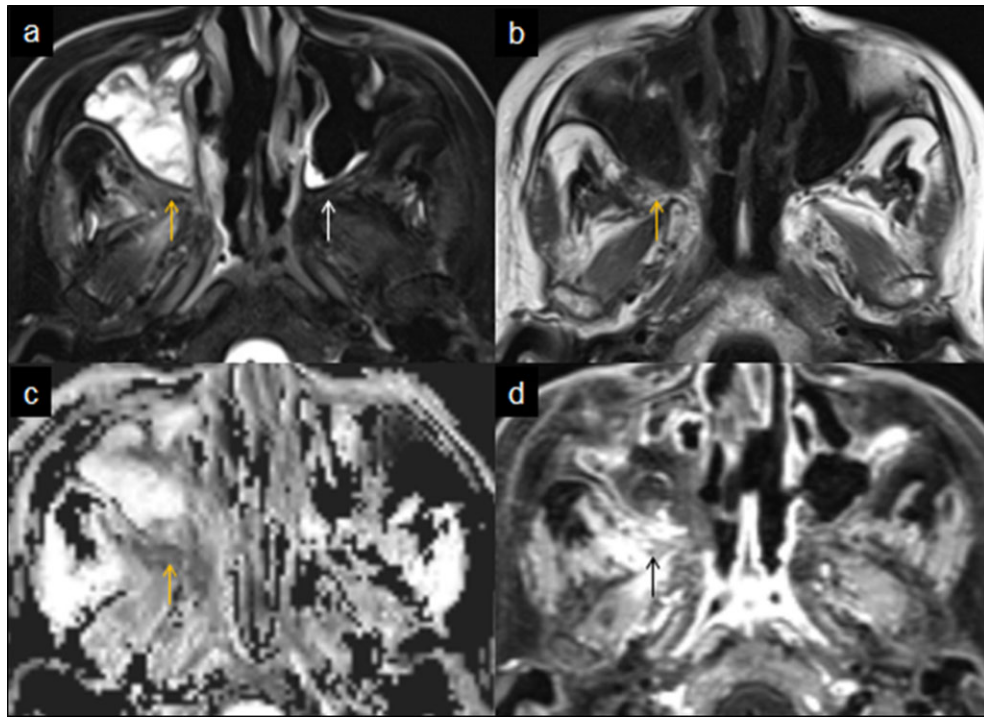


**Figure 7.** ROCM with right lower motor neuron facial palsy. Soft tissue infiltration and fat stranding is seen in right pterygopalatine fossa appearing as (a) hyperintense on axial T2 Dixon fat-saturation image (yellow arrow), (b) hypointense on T1W image (yellow arrow), (c) hypointense on ADC image suggestive of diffusion restriction (yellow arrow), and (d) heterogenous enhancement on axial T1W fat-saturation post-contrast MR image (black arrow). The contralateral normal pterygopalatine fossa is marked by a white arrow in (a). Additionally, right masticator muscles appear hyperintense in (a).

assemblies of clinico-imaging presentations.<sup>15</sup> Previously overlooked environmental factors specific to India were important contributors to the country's ROCM outbreak which is spread of fungal spores, mainly through fumes generated from the burning of Mucorales-rich biomass, like cow dung and crop stubble could have caused extensive environmental exposure in the context of a large population of highly vulnerable patients with diabetes mellitus and COVID-19.<sup>16</sup> The massive outbreak of ROCM fueled by the second wave of the SARS-CoV-2 pandemic in India provided an opportunity to investigate the presenting clinical and imaging manifestations of ROCM in great detail. This report relates to the presenting clinical and imaging findings in a series of patients seen during the outbreak in a single-center, which offered multidisciplinary care. Complete loss of vision with no light perception in one eye was a common finding, observed in nearly three-quarters of the subjects. Likewise, a frozen eye with complete ophthalmoplegia, proptosis, and congestion, was a characteristic, and common finding. Apart from the optic and oculomotor nerve palsies, the trigeminal nerve or its branches (in nearly one-third) and the facial nerve (in one-half) were found to be clinically affected, albeit mostly unilaterally (Figs. 4a–b and 5a–d). In none of the subjects were the imaging findings confined to the nasal cavity alone. A unilaterally involved maxillary sinus was most commonly noted followed closely by ethmoidal sinus disease. A combination of maxillary, ethmoidal, and sphenoidal sinus disease was observed in 33% of cases.

Our observations indicate that a complete ophthalmoplegia in the form of a frozen (i.e., fixed and immobile), proptosis and congested eye with or without vision loss, especially when associated with imaging evidence of ethmoidal or maxillary sinusitis and in the setting of the several well-described

risk factors is virtually diagnostic of ROCM. The direction of proptosis is also relevant and might provide a hint to the predominant paranasal sinus involved (Fig. 3a–d). A vertical shift was observed in four cases with predominant maxillary sinus involvement and laterally-directed proptosis in three subjects with predominant ethmoidal sinusitis.

Of note, orbital or periorbital pain was conspicuous by its absence in 30 cases in the current series. Painless ophthalmoplegia has seldom been reported previously in the setting of ROCM.<sup>17</sup> Rather, pain has been previously reported in ROCM at a variety of sites including the face opposite to the maxillary sinus(es), the bridge of the nose occasioned by ethmoidal sinusitis or the vertex of the cranium as in sphenoidal sinus or intracranial mucormycosis.<sup>18,19</sup> Pain might also occur over the orbit as observed in six subjects in this report. An orbital compartment syndrome was observed in two subjects with orbital pain in this study.<sup>20</sup> Orbital pain might also occur because of the involvement of several sensory nerves in the superior orbital fissure, orbital periosteum, and muscle inflammation. However, we could not find any association between the presence of orbital pain and the location of disease with respect to anatomical segments within the superior orbital fissure.

An ipsilateral lower motor neuron facial palsy was observed in 19 (61%) subjects in the current study. This proportion is higher than the frequency reported in previous studies.<sup>21,22</sup> Indeed, facial nerve palsy has been reported in few isolated cases only.<sup>23,24</sup> In these reports, the facial nerve appears to be involved in the bony facial canal, presumably as a result of chronic granulomatous skull base osteomyelitis, an indolent presentation of ROCM.<sup>25</sup> We, however, did not observe erosion of the bony facial canal assessed on CT in 19 subjects

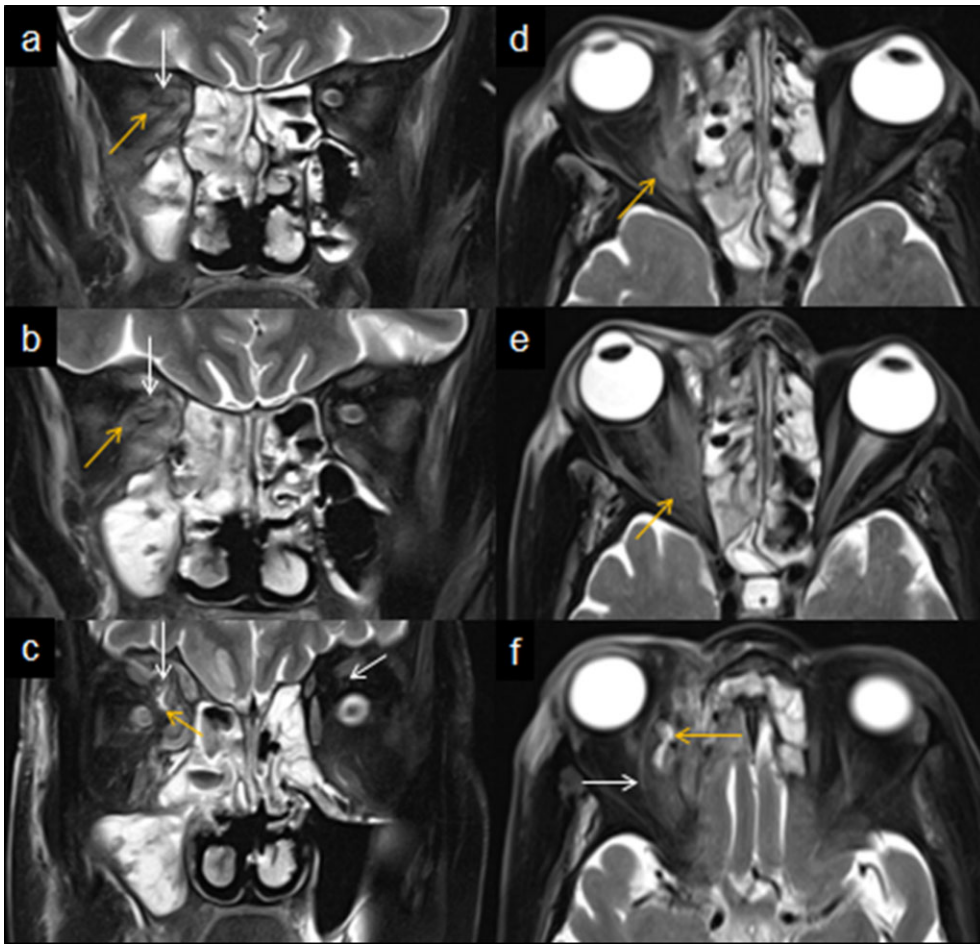


**Figure 8.** ROCM with complete right ophthalmoplegia. Segments of superior orbital fissure are shown in coronal T2 fat-saturation MR images from posterior to anterior (a–c), with corresponding axial T2 fat-saturation MR images from inferior to superior (d–f). Hyperintense soft tissue infiltration (yellow arrows) is seen in the fat inferolateral to optic nerve (white arrows) in (a), (b), (d), (e) showing involvement of intra-annular middle segment of superior orbital fissure and orbital apex. Images (c) and (f) demonstrate hyperintense soft tissue (yellow arrows) in the fat surrounding superior ophthalmic vein (white arrows) indicating involvement of superolateral extra-annular segment of the superior orbital fissure. Optic nerve is marked with white arrows in (a) and (b). Superior ophthalmic vein is marked with white arrows in (c) and (f). Normal fat is seen surrounding the optic nerve and superior ophthalmic vein on the left side.

with a clear documented facial nerve palsy. Hence, we hypothesized that the facial nerve involvement was caused by the neural spread of the fungus along the Vidian nerve (or the greater superficial petrosal nerve) in the Vidian canal<sup>26</sup> to the geniculate ganglion. This nerve is a branch of the facial nerve distal to the geniculate ganglion and travels in the bony Vidian canal to the pterygopalatine ganglion located in the pterygopalatine fossa.<sup>27,28</sup> Perineural spread of mucor is well-documented and may underline the high frequency of facial nerve palsy in SARS-CoV-2-associated ROCM.<sup>29</sup> In the current series, greater size and intensity of enhancement of the geniculate ganglion of the facial nerve ipsilateral to the side of the lower motor neuron facial palsy was observed in 7 (64%) out of 11 subjects in whom post-contrast MRI was performed. Moreover, soft tissue extension to, and/or fat stranding in the pterygopalatine fossa was observed in 18/20 (90%) patients undergoing MRI; of these, 14 had an ipsilateral facial palsy.<sup>30</sup> Both imaging features might be construed as indirect evidence to support perineural spread from the pterygopalatine fossa to the facial nerve.

The absence of bony canal involvement in subjects with facial palsy and otherwise in this series deserves comment. Skull

base osteomyelitis and bony involvement are usually absent in the early stage and occur late in ROCM.<sup>31,32</sup> This is because the angio-invasive fungus rapidly permeates through perivascular channels and bony destruction follows indolently. Acute invasive mucormycotic sinusitis presenting with skull base osteomyelitis is rare but may occur in immunocompromised patients.<sup>31</sup> Accordingly, skull base osteomyelitis was demonstrated in only 5 (14%) subjects in the current study.

Complete loss of vision, mostly unilateral was observed early in nearly three-quarters of the subjects. Distinct from this, four patients had only partial loss of vision in one or both eyes. One of the causes for complete loss of vision could be complete central retinal artery occlusion (CRAO), a finding that was demonstrated in 11 (48%) of 23 subjects in whom funduscopy was undertaken.<sup>33</sup> On MRI, long segments of infarcted tissue in the posterior portions of the optic nerves were noted in 9 (82%) of the 11 patients with central retinal artery occlusion. These findings are compatible with a diagnosis of PION and are distinct from the MR imaging findings in anterior ischemic optic neuropathy (AION), in which the abnormalities might be confined to the optic disc.<sup>34</sup> AION is manifested by pale swelling of the optic disk and peripapillary

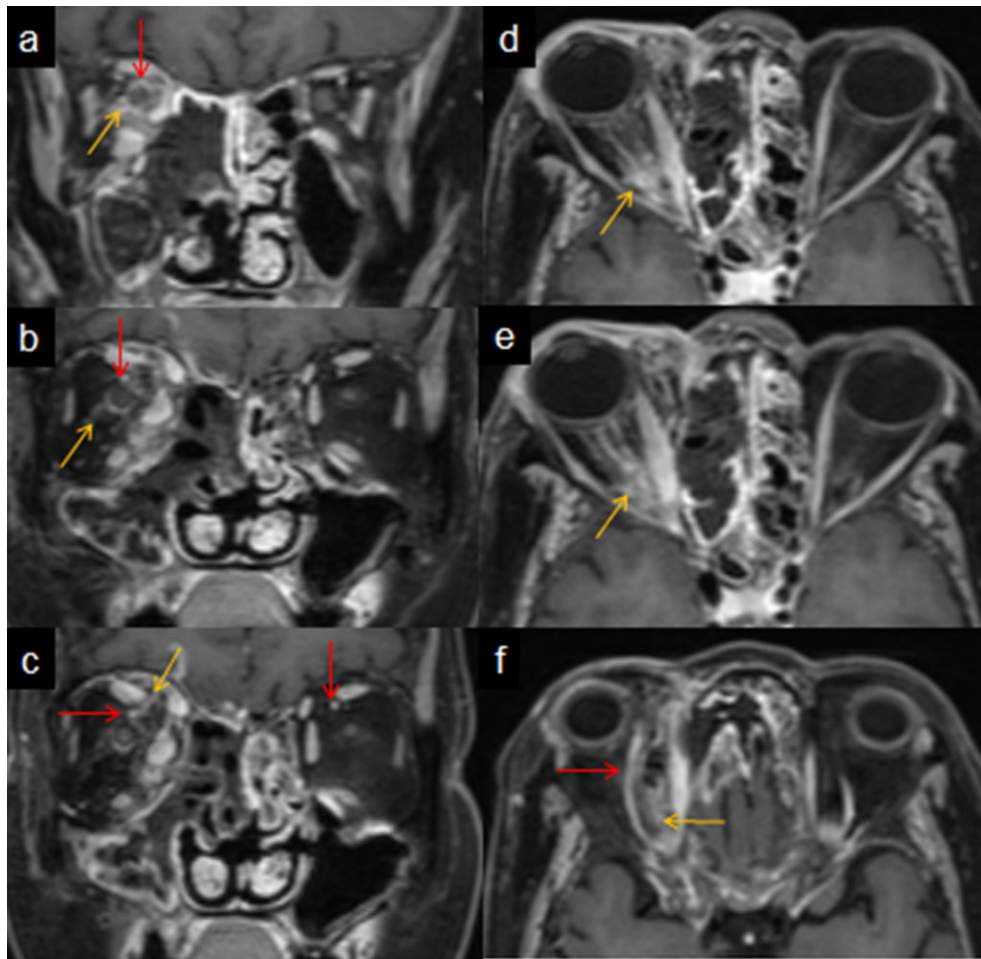


**Figure 9.** ROCM with complete ophthalmoplegia right side, same case as in Figure 5. Segments of superior orbital fissure are shown in coronal T1 fat saturation post contrast MR images from posterior to anterior (a–c), with corresponding axial T1 fat saturation post contrast images from inferior to superior (d–f). Optic nerve is marked with red arrows in (a and b). Superior ophthalmic vein is marked with red arrows in (c and f). Heterogenous post contrast enhancement within the soft tissue infiltration (yellow arrows) is seen in the fat inferolateral to optic nerve (red arrows) in (a), (b), (d), (e) showing involvement of intra-annular middle part of superior orbital fissure and orbital apex. (c), (f) images show heterogeneously enhancing soft tissue (yellow arrows) in the fat surrounding superior ophthalmic vein (red arrows), showing involvement of superolateral extra-annular part of superior orbital fissure. Normal fat is seen surrounding the optic nerve and superior ophthalmic vein on contralateral side.

hemorrhages. PION is a retrobulbar involving the optic nerve and or optic chiasm, but the optic disk is not initially swollen. Presumably, the posteriorly-located imaging lesions within the optic nerve reflect occlusion of the pial branches of the ophthalmic artery on account of the angio-invasive nature of mucor.<sup>35</sup> The combination of CRAO and PION in many of the cases in this series probably represents an entire orbital infarction pattern.<sup>36</sup> Other plausible causes for vision loss might include optic neuritis<sup>37</sup> and involvement of optic nerves as a manifestation of orbital apex syndrome due to invasive fungal sinusitis.<sup>38</sup> Direct compression of the optic nerves has been reported due to a mass in the sphenoid sinus, which was contiguous with the optic nerve.<sup>39</sup>

In the patient sample, microbiological diagnosis of ROCM was established through a combination of microscopic and histopathological examinations in all. Conventional laboratory diagnosis of mucormycosis comprises of microscopic examination, histopathological examination, and culture sensitivity. KOH wet mounts or calcofluor stains under fluorescent microscopy demonstrate the characteristic fungal hyphae to provide a likely diagnosis. As a rule, however, histopathological examination with routine hematoxylin and eosin and pe-

riodic acid-Schiff stains are confirmatory. The typically broad, aseptate, and with wide-angle branching of mucor can be differentiated from the narrow septate hyphae of *Aspergillus*. Besides this, culture methods are helpful in identifying the species and testing antifungal drug sensitivity with the caveats of time delay, low sensitivity, and risk of contamination.

Our study was not without limitations. An appalling and complete shortage of amphotericin B across India during the period of admission of these subjects led to amendments in the treatment approaches and could have impacted the outcome, which, accordingly, we opted not to present in this report. Many subjects in the study were evaluated with CT alone, while others underwent MR examinations or a combination of CT and MR imaging. The choice of imaging was really determined by the SARs-CoV-2-positivity status as a positive RT-PCR test led to triage to a stand-alone CT facility reserved for COVID-19-infected patients. On the other hand, MRI examination could be performed only in SARs-Cov-2 RT-PCR negative subjects as this is a lone and busy facility for the entire hospital. Hence, the analysis presented is based on a mix of CT and MR images. Lastly, any attempt to compare the clinical and radiological profile of COVID-19-associated ROCM

and otherwise ideally should involve an exposed-unexposed design, which would be challenging as ROCM incidence has numerically declined with the subsidence of the second SARS-CoV-2 wave in India.

In conclusion, our analysis of clinical and radiological presentations of COVID-19-associated ROCM demonstrates its likeness to native ROCM in terms of disease characteristics. Of note, however, a milder spectrum of disease such as isolated nasal disease eluded our sample of subjects, perhaps conforming to a rather rapid and aggressive course of the disease. The pattern of paranasal sinus involvement is only slightly different from that reported in previous studies and the spectrum of intracranial involvement matches with both other reports of COVID-19-associated and native ROCM. However, some of the distinctive features brought out in this report serve as important take-home points. These include the complete loss of vision in a large number of subjects with corresponding imaging characteristics of posteriorly located long-segment ischemic optic neuropathies identified on diffusion-weighted imaging of the optic nerves, the significance of directional predominance of proptosis, the absence of orbital and periorbital pain in many subjects and the large proportion with lower motor neuron facial palsy. Corresponding to the observation of unilateral lower motor neuron facial palsy are the characteristic imaging findings relating to the type, intensity, and pattern of enhancement of the ipsilateral geniculate ganglion, probably consistent with a perineural spread of the fungus from the pterygopalatine fossa to the geniculate ganglion via the greater superficial petrosal nerve. These are some of the unique findings brought out in this study and it would be interesting to note if similar findings are also seen in the period following the waning of the SARS-CoV-2 pandemic.

## Funding

None.

## Authors' contributions

G.S., K.S., A.A., and M.M. conceived the study; A.M. and N.S. undertook the descriptive analysis and drafted the paper; all others critically reviewed, revised the manuscript, and provided substantial intellectual input.

## Disclosures

None

## Declaration of interest

There is no conflict of interest to declare.

## References

- Vallinayagam M, Balla SC, Krishnagopal S, Karthikeyan P, Sowmya S. Rhino-orbital Mucormycosis Manifesting as Orbital Apex Syndrome with CRAO in An Immunocompetent Patient. *DJO*. 2019; 30: 58–61.
- Cornely OA, Alastruey-Izquierdo A, Arenz D et al. Global guideline for the diagnosis and management of mucormycosis: an initiative of the European Confederation of Medical Mycology in cooperation with the Mycoses Study Group Education and Research Consortium. *Lancet Infect Dis*. 2019; 19: e405–e421.
- Rees VJR, Pinner RW, Hajjeh RA. The epidemiological features of invasive mycotic infections in the San Francisco Bay area, 1992–1993: results of population-based laboratory active surveillance. *Clin Infect Dis*. 1998; 27: 1138–1147.
- Prakash H, Chakrabarti A. Global epidemiology of mucormycosis. *J Fungi*. 2019; 5: 26.
- Rao V, Arakeri G, Madikeri G, Shah A, S Oeppen R, A Brennan P. Post-COVID mucormycosis in India: a formidable challenge. *Br J Oral Maxillofac Surg*. 2021;10.1016/j.bjoms.2021.06.013
- Singh G, Vishnu VY. Neurological manifestations of rhino-ocular-cerebral mucormycosis in the COVID-19 era. *Nat Rev Neurol*. 2021; 17: 657–658.
- Ismaiel WF, Abdelazim MH, Eldsoky I, Ibrahim AA, Alsobky ME, Zafan E, Hasan A. The impact of COVID-19 outbreak on the incidence of acute invasive fungal rhinosinusitis. *Am J Otolaryngol*. 2021; 42: 103080.
- Farias LABG, Damasceno LS, Bandeira SP, Barreto FKA, Leitão TDMJS, Cavalcanti LPG. COVID-19 Associated Mucormycosis (CAM): should Brazil be on alert? *Rev Soc Bras Med Trop*. 2021; 54: e04102021.
- Singh AK, Singh R, Joshi SR, Misra A. Mucormycosis in COVID-19: a systematic review of cases reported worldwide and in India. *Diabetes Metab Syndr*. 2021; 15: 102146.
- Clinical Microbiology Procedure Handbook, Chief in editor Isenberg H.D., *Albert Einstein College of Medicine*, New York, Publisher ASM (American Society for Microbiology), Washington DC.
- Therakathu J, Prabhu S, Irodi A, Sudhakar SV, Yadav VK, Rupa V. Imaging features of rhinocerebral mucormycosis: a study of 43 patients. *Egypt J Radiol Nucl Med*. 2018; 49: 447–452.
- Li H, Zhou H, Sun J, Wang H, Wang Y, Wang Z et al. Optic neuritis and its association with autoimmune diseases. *Front Neurol*. 2021; 11: 627077.
- Al-Noury K, Lotfy A. Normal and pathological findings for the facial nerve on magnetic resonance imaging. *Clin Radiol*. 2011; 66: 701–707.
- Lieber S, Fernandez-Miranda JC. Anatomy of the orbit. *J Neurol Surg B Skull Base*. 2020; 81: 319–332.
- Lone PA, Wani NA, Jehangir M. Rhino-orbito-cerebral mucormycosis: magnetic resonance imaging. *Indian J Otol*. 2015; 21: 215–218.
- Skaria J, John TM, Varkey S, Kontoyiannis DP. Are unique regional factors the missing link in India's COVID-19-Associated mucormycosis crisis?. *mBio*. 2022; 13: e0047322.
- Balch K, Phillips PH, Newman NJ. Painless orbital apex syndrome from mucormycosis. *J Neuroophthalmol*. 1997; 17: 178–182.
- Klimko N, Khostelidi S, Shadrivova O, Volkova A, Popova M, Uspenskaya O et al. Contrasts between mucormycosis and aspergillosis in oncohematological patients. *Med Mycol*. 2019; 57: S138–S144.
- Song Y, Qiao J, Giovanni G, Liu G, Yang H, Wu J, Chen J. Mucormycosis in renal transplant recipients: review of 174 reported cases. *BMC Infect Dis*. 2017; 17: 283.
- Werthman-Ehrenreich A. Mucormycosis with orbital compartment syndrome in a patient with COVID-19. *Am J Emerg Med*. 2021; 42: 264.e5–264.e8.
- Sen M, Honavar SG, Bansal R, Sengupta S, Rao R, Kim U et al. Epidemiology, clinical profile, management, and outcome of COVID-19-associated rhino-orbital-cerebral mucormycosis in 2826 patients in India – Collaborative OPAI-IJO Study on Mucormycosis in COVID-19 (COSMIC), Report 1. *Indian J Ophthalmol*. 2021; 69: 1670–1692.
- Patel A, Kaur H, Xess I et al. A multicentre observational study on the epidemiology, risk factors, management and outcomes of mucormycosis in India. *Clin Microbiol Infect*. 2020; 26: 944. e9–944. e15.
- Vishnu Swaroop Reddy N, Natti RS, Radha T, Sharma M, Chintham M. Skull base mucormycosis in an immunocompetent

- patient: a case report and literature review. *Indian J Otolaryngol Head Neck Surg.* 2019; 71: 140–143.
24. Shah V, Ganapathy H, Gopalakrishnan R, Geetha N. A rare case of facial palsy due to mucormycosis. *Int J Otolaryngol Head Neck Surg.* 2015; 4: 224–228.
  25. Harrill WC, Stewart MG, Lee AG, Cernoch P. Chronic rhinocerebral mucormycosis. *Laryngoscope.* 1996; 106: 1292–1297.
  26. Osawa S, Rhoton AL, Jr, Seker A, Shimizu S, Fujii K, Kassam AB. Microsurgical and endoscopic anatomy of the vidian canal. *Neurosurgery.* 2009; 64: 385–411.
  27. Chhabda S, Leger DS, Lingam RK. Imaging the facial nerve: a contemporary review of anatomy and pathology. *Eur J Radiol.* 2020; 126: 108920.
  28. Singh AK, Bathla G, Altmeyer W, Tiwari R, Valencia MP, Bazan C, 3rd, Tantiwongkosi B. Imaging spectrum of facial nerve lesions. *Curr Probl Diagn Radiol.* 2015; 44: 60–75.
  29. McLean FM, Ginsberg LE, Stanton CA. Perineural spread of rhinocerebral mucormycosis. *AJNR Am J Neuroradiol.* 1996; 17: 114–116.
  30. Raab P, Sedlacek L, Buchholz S, Stolle S, Lanfermann H. Imaging patterns of Rhino-orbital-cerebral mucormycosis in immunocompromised patients: when to suspect complicated mucormycosis. *Clin Neuroradiol.* 2017; 27: 469–475.
  31. Verma RK, Angrish P, Mitra S, Rudramurthy SPM. Varied presentation of mucormycotic skull base osteomyelitis: series of three cases. *J Korean Skull Base Soc.* 2021; 16.
  32. Devireddy SK, Kishore Kumar RV, Gali R, Kanubaddy SR, Dasari MR, Akheel M. Mucormycotic skull base osteomyelitis: a case report. *J Oral Maxillofac Surg Med Pathol.* 2014; 26: 336–339.
  33. Bawankar P, Lahane S, Pathak P, Gonde P, Singh A. Central retinal artery occlusion as the presenting manifestation of invasive rhino-orbital-cerebral mucormycosis. *Taiwan J Ophthalmol.* 2020; 10: 62–65.
  34. Paul B, McElvanney AM, Agarwal S et al. Two rare causes of posterior ischaemic optic neuropathy: eosinophilic fasciitis and Wegener's granulomatosis. *Br J Ophthalmol.* 2002; 86: 1066–1068.
  35. Ghuman MS, Kaur S, Bhandal SK, Ahluwalia A, Saggar K. Bilateral optic nerve infarction in rhino-cerebral mucormycosis: a rare magnetic resonance imaging finding. *J Neurosci Rural Pract.* 2015; 6: 403–404.
  36. Borruat FX, Bogousslavsky J, Uffer S, Klainguti G, Schatz NJ. Orbital infarction syndrome. *Ophthalmology.* 1993; 100: 562–568.
  37. Kahloun R, Abroug N, Ksiaa I et al. Infectious optic neuropathies: a clinical update. *Eye Brain.* 2015; 7: 59–81.
  38. Lee DH, Yoon TM, Lee JK, Joo YE, Park KH, Lim SC. Invasive fungal sinusitis of the sphenoid sinus. *Clin. Exp. Otorhinolaryngol.* 2014; 7: 181–187.
  39. Sano T, Kobayashi Z, Takaoka K et al. Retrobulbar optic neuropathy associated with sphenoid sinus mucormycosis. *Neurol Clin Neurosci.* 2018; 6: 146–147.